Feature extraction method of hyperspectral scattering images for prediction of total viable count in pork meat

Tao Feifei, Peng Yankun*, Li Yongyu

(*College of Engineering, China Agricultural University, Beijing 100083, China*)

Abstract: This study aimed to investigate the capabilities of hyperspectral scattering imaging in tandem with Gaussian function, Exponential function and Lorentzian function for rapid and nondestructive determination of total viable count (TVC) in pork meat. Two batches of fresh pork meat was purchased from a local market and stored at 10°C for 1-9 d. Totally 60 samples were used, and several samples were taken out randomly for hyperspectral scattering imaging and conventional microbiological tests on each day of the experiments. The functions of Gaussian, Exponential and Lorentzian were employed to model the hyperspectral scattering profiles of pork meat, and good fitting results were obtained by all three functions between 455 nm and 1 000 nm. The Lorentzian function performed best for fitting the hyperspectral scattering profiles of pork meat compared with other functions. Both principal component regression (PCR) and partial least squares regression (PLSR) methods were performed to establish the prediction models. Among all the developed models, the models developed using parameters C_E (scattering width parameter of Exponential function) and C_L (scattering width parameter of Lorentzian function) by PLSR method gave superior results for predicting pork meat TVC, with R_V and RMSEV of 0.92, 0.59 log CFU/g, and 0.91, 0.61 log CFU/g, respectively. In addition, based on the improved hyperspectral scattering system, parameter *c* which represented the scattering widths in all three functions gave more accurate prediction results, regardless of the modeling methods (PCR or PLSR). The obtained results demonstrated that hyperspectral scattering imaging combined with the presented data analysis algorithm can be a powerful tool for evaluating the microbial safety of meat in the future.

Keywords: hyperspectral scattering imaging, pork meat, total viable count, Lorentzian function, Gaussian function, Exponential function

DOI: 10.3965/j.ijabe.20150804.1559

Citation: Tao F F, Peng Y K, Li Y Y. Feature extraction method of hyperspectral scattering images for prediction of total viable count in pork meat. Int J Agric & Biol Eng, 2015; 8(4): 95－105.

1 Introduction

Pork meat is a commercially important and widely consumed muscle food in the world; therefore, the assurance of its safety is of utmost importance. Sofos[1] reported microbial hazard to be one of the major challenges to meat safety in the 21st century. The microbiological quality of meat mainly depends on the physiological status of the animal at slaughter, the spread of contamination during slaughter and processing, the temperature and other conditions of storage and distribution[2]. Total viable count (TVC) of bacteria is an important microbiological indicator for the sanitary quality and safety evaluation of meat. It is a quantitative sanitary standard to identify the process conditions and meat contamination[3-4]. Moreover, TVC can also be a useful indicator to predict the shelf life of meat and distinguish spoilage[5]. However, the existing methods for detection of bacteria in meat are mainly based on plate culturing, ATP bioluminescence, enzyme-linked immunosorbent assay (ELISA), polymerase chain reaction (PCR), etc[6-8]. An obvious drawback with the common plate culturing method is the long detection time

Received date: 2014-12-29 **Accepted date:** 2015-07-06

Biographies: Tao Feifei, PhD, Postdoctorate. Research area: Optical technology for rapid and nondestructive evaluation of food quality and safety. Email: feiftao@gmail.com. **Li Yongyu**, PhD, Associate Professor. Research area: Optical technology for rapid and nondestructive evaluation of food quality and safety. Email: yyli@cau.edu.cn.

***Corresponding author: Peng Yankun,** PhD, Professor, College of Engineering, China Agricultural University. Research area: Optical technology for rapid and nondestructive evaluation of food quality and safety. Mailing address: 17 Qinghua East Road, Haidian, Beijing 100083, China. Email: ypeng@cau.edu.cn. Tel: +86-10-62737703, Fax: +86-10-62737997.

required for colony formation[9]. Other newly emerging techniques may have successfully shortened the detection time; however, they still could not meet the requirements of meat industries for real-time and in/on-line detection of bacteria, because of them being destructive to samples.

Among current emerging technologies, optic-based methods were reported to have the greatest potential for on-line application[10,11]. Hyperspectral imaging technique is a new rapidly growing technique that integrates spectroscopic and imaging techniques together for providing both spectral and spatial information of the object simultaneously. Recently, considerable studies have been reported on evaluation of food quality and safety attributes using hyperspectral imaging technique[12-28]. In the area of hyperspectral imaging, hyperspectral scattering imaging can be considered to be one branch, as it is based on the light backscattering imaging (LBI) system which could cover both light scattering and absorption information within samples. Light scattering is commonly reported to be due to the physical characteristics (e.g., particle size, cellular structure and density) of the tissue, while light absorption is related to the chemical constituents. During the process of meat spoilage, not only the bacterial loads and chemical ingredients undergo changes, but also the microstructure of meat can be different. Therefore, it is reasonable to apply hyperspectral scattering imaging to quantify meat TVC changes during storage, as it can cover both the differences in light scattering and absorbance.

However, a critical problem encountered in the application of hyperspectral scattering imaging is to analyze and model hyperspectral scattering profiles. Previously, Peng and Lu[29] exploited Lorentzian function, Gaussian function and Exponential function to model the multispectral scattering profiles of apple fruits, and concluded that Lorentzian function could yield the best fitting results to the scattering profiles of apple fruits. Subsequently, Peng et al.[30] continued to apply different forms of Lorentzian function and Gompertz function to analyze the characteristics of multispectral scattering profiles of apple fruits, and their results showed that Gompertz function performed better for predicting apple quality attributes than Lorentzian function, although with a little bit lower fitting coefficients. Recently, Zhu et al.[31] reported using a generalized Gaussian function coupled with mean reflectance (GGD-mean) to describe the hyperspectral scattering profiles of 'Golden Delicious' apples in the spectral region of 500-1 000 nm, and indicated that GGD-mean model could yield better results for predicting fruits firmness and SSC than Lorentzian function. In the field of evaluating meat quality and safety by hyperspectral scattering imaging, studies have been reported on exploiting Lorentzian function and Gompertz function to analyze the scattering profiles of beef and pork meat[18,22,24-27]. However, to our knowledge, the capabilities of Gaussian function and Exponential function in modeling the hyperspectral scattering profiles of meat are still unknown now. Therefore, the objectives of the present study are: (1) to explore the capabilities of Gaussian function and Exponential function in modeling the hyperspectral scattering profiles of pork meat; (2) to investigate the effectiveness of the extracted Gaussian and Exponential parameters in predicting pork meat TVC, and also compare their modeling results with those by Lorentzian parameters; (3) to test the capabilities of the improved hyperspectral scattering imaging system in detection of the bacterial contamination of pork meat.

2 Materials and methods

2.1 Sample preparation

Two batches of fresh pork meat (*Longissimus dorsi muscle*) were purchased from a local supermarket on two different days and immediately transported to the lab under refrigeration. Totally 60 pork meat samples were prepared by trimming into the size of 9 cm×5 cm×2.5 cm (length × width × thickness) uniformly, and then tray-packaged with polyethylene (PE) film covering above. All samples were placed orderly and stored at 10°C for 1-9 d. Several samples were taken out randomly on each day of the experiment for hyperspectral imaging and reference microbiological tests.

2.2 Hyperspectral scattering imaging system

A laboratory VIS/NIR hyperspectral scattering imaging system in the spectral range of 400-1 100 nm

was used. Compared to our previous study[25], this system was enhanced by improving the charge coupled device (CCD) lens to an adjusted one that allowing over 80% light transmittance in the covered near-infrared region.

The hyperspectral imaging system mainly consisted of a high-performance back-illuminated 12-bit charge coupled device (CCD) camera (Sensicam QE, PCO AG, Kelheim, Germany), an imaging spectrograph (ImSpector V10E, Spectral Imaging Ltd., Oulu, Finland), an illumination unit (Oriel Instruments, Stratford, USA) equipped with optical fiber, a laser displacement sensor (GV-H45, Keyence Corp., Shanghai, China), and a computer supported with a data acquisition and control software (Camera control Kit V2.19, the Cooke Corp., Germany). The optical fiber was used to form the point light for use in the scattering imaging system, with a diameter of 5 mm. The system worked in a line scanning mode, and all scans were obtained at a position of 3 mm off the incident light center to avoid the signal saturation on CCD detector. The resolution of the imaging system was 2.8 nm spectrally with a 0.74 nm interval, and spatially less than 9 μm. In addition, in order to minimize the effect of ambient light, the imaging system was enclosed in a shield box.

2.3 Acquisition of hyperspectral images

In order to eliminate the dark current effect of the imaging system, the dark image was first obtained by covering the camera lens before imaging for each sample. Sample surface with no visible fat or connective tissue was selected for imaging. For each sample, four lines in the middle of the sample were selected for imaging, and the gap between two adjacent lines was around 0.5 cm if no visible fat or connective tissue existed there. The gap of 0.5 cm was not necessary, if visible fat or connective tissue existed. For each imaging, four images were averaged to one automatically by setting the camera working parameter thus, 16 hyperspectral images were acquired for each sample actually. Before each imaging, the object distance was first measured by the laser displacement sensor, and then kept to the set distance by adjusting the vertical translation stage.

The original hyperspectral images were of 1 376× 1 040 (spatial × spectral) pixels, and 2×2 binning was performed to improve the signal-to-noise ratio (SNR). Therefore, the resulting images were of 688×520 (spatial × spectral) pixels, which were saved in TIFF format for further analysis.

2.4 Microbiological analyses

After acquisitions of hyperspectral images, the microbiological tests were performed to determine the reference TVCs in pork meat according to GB/T 4789.2-2010. First, 25 g samples were transferred aseptically into 225 mL sterilized 0.85% saline solution, and homogenized (10 000 r/min) in a homogenizer (JT-C, Luohe Jintian Test Equipment Institute, Luohe, China) for 60 s at room temperature. Then, 10-fold serial dilutions were prepared with 0.85% saline solution and duplicate 1 mL samples of 2 or 3 appropriate dilutions were mixed with the liquid Plate Count Agar (Beijing Aoboxing Bio-tech Co. Ltd, Beijing, China). The agar plates were left on the bench for at least 15 min to solidify and were then incubated at 37°C for 48 ± 2 h. The number of total bacteria in each sample was determined by counting the number of colony forming units (CFUs). The data of pork meat TVCs were calculated according to GB 4789. 2-2010. Finally, the TVC data were log-transformed, and expressed in log CFU/g for further analysis.

2.5 Data analysis method

Figure 1 presents the data processing procedures employed in this work, and the detailed data analysis method for each step is described in the following sections.

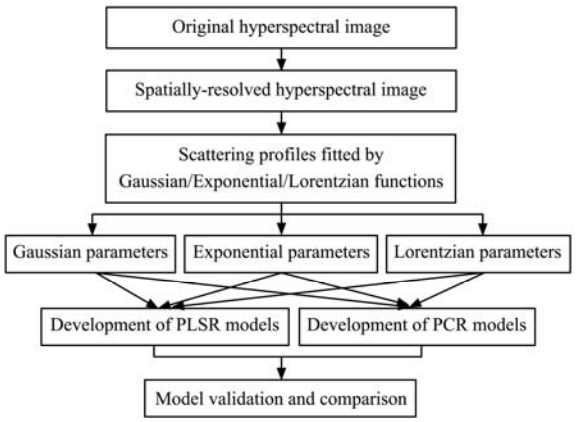

Figure 1 Schematic diagram of data processing routines

2.5.1 Spatially-resolving of hyperspectral image

Hyperspectral image contains three-dimensional (3-D)

information of the object, and therefore it should first be unfolded and restructured into a 2-D matrix in order to apply the chemometric techniques. In this work, the spatially-resolving method was employed to analyze the images[18,22,24]. The spatially-resolved hyperspectral image, essentially are the scattering profiles of the object at contiguous wavelengths. In this work, three functions including Gaussian function, Exponential function and Lorentzian function were applied to extract the scattering characteristics of pork meat.

Gaussian function, Exponential function and Lorentzian function are shown in Equations (1)-(3), respectively.

$$R = a_G + b_G e^{-0.5\left(\frac{z}{c_G}\right)^2} \quad (1)$$

$$R = a_E + b_E e^{-\left(\frac{|z|}{c_E}\right)} \quad (2)$$

$$R = a_L + \frac{b_L}{1+\left(\frac{z}{c_L}\right)^2} \quad (3)$$

where, R is the light intensity in CCD Count; z is the distance from the detected position to the light incident center in pixel; a_G, a_E, and a_L are the asymptotic values of light intensity in Gaussian, Exponential and Lorentzian functions, respectively; b_G, b_E and b_L are the peak values of light intensity in Gaussian, Exponential and Lorentzian functions, respectively; c_G is the scattering width at $0.61\times b_G$ in Gaussian function; c_E is the scattering width at $0.37\times b_E$ in Exponential function; and c_L is the scattering width at $0.5\times b_L$ in Lorentzian function.

All the curve-fitting procedures were performed in Matlab 7.0 software (Mathworks, Natick, USA) based on the least-squares principle, and the fitting results were evaluated by the correlation coefficients (R) between the original scattering profiles and the fitted function curves. The higher R is, the more accurate the fitting is. By the procedure of curve fitting, the Gaussian, Exponential and Lorentzian function parameters can be obtained, respectively.

2.5.2 Model calibration and validation

Principal component analysis (PCA) and partial least squares (PLS) are two full-spectrum and factor analysis methods based on multivariate calibration that have received considerable attentions in the chemometric literatures[32-35]. Using the extracted function parameters, both principal component regression (PCR) and partial least squares regression (PLSR) methods were employed in this work to establish the quantitative models for prediction of pork meat TVC.

PCA is a well-known technique for reducing a multidimensional data set to its most dominant features, and expresses the total variation in the data set in only a few principal components (PCs). These PCs are orthogonal, so that the data set presented on these axes are uncorrelated with each other[36]. In PCA, the independent data matrix (X, function parameter in this case) is decomposed into two matrices, T and P, such that $X = TP^T$. Where T is the "score" matrix, which represents the position of the sample in the new coordinate system (PCs coordinate system); P is the "loading" matrix, whose columns describe how the new axes, that is the PCs, are built from the old axes. Therefore, each spectrum will have its own unique set of scores, and a spectrum can be represented by its PCA scores in the factor space instead of intensities in the wavelength space[37].

In PLS, the decomposition is performed in a slightly different fashion. Instead of first decomposing the spectral matrix into a set of scores and loadings, and regress for them against the dependent variable (Y, reference TVC value in this case) as a separate step, PLS actually uses the information in Y during the decomposition process. The main idea of PLS is to get as much information in Y as possible into the first few loading vectors. The first latent variable (LV) conveys the largest amount of information, followed by the second LV and so forth.

To evaluate the capabilities of the established models in predicting pork meat TVC, the statistical criteria, including correlation coefficient of the calibration set (R_C), root mean squared error of the calibration set (RMSEC), correlation coefficient of the validation set (R_V) and root mean squared error of the validation set (RMSEV) were computed. The higher Rv and the lower RMSEV is, the better predictability the model has.

3 Results and discussion

3.1 Results of microbiological analysis

The statistical data of pork meat TVC of all 60 samples were calculated and the results were shown in Table 1. From Table 1, it could be seen that the minimum TVC of all tested samples was 4.38 log CFU/g and the maximum value was 9.29 log CFU/g, with the mean value and standard deviation (SD) of 6.98 log CFU/g and 1.45 log CFU/g, respectively. These statistical data indicated that a wide range of meat TVC values was covered, and it could represent the complete process of microbial spoilage of pork meat.

In addition, as the samples were divided into calibration and validation sets in the following section for model development and evaluation, the statistical data was also calculated for each of them and the results were shown in Table 1 together.

Table 1 Descriptive statistics of reference pork meat TVCs (in log CFU/g)

Data set	Sample number	Minimum	Maximum	Mean	SD
Total set	60	4.38	9.29	6.98	1.45
Calibration set	45	4.39	9.29	6.97	1.45
Validation set	15	4.38	8.99	7.03	1.45

3.2 Analysis of hyperspectral data

3.2.1 Spatially-resolving of hyperspectral image

Figure 2 shows the hyperspectral scattering image of pork meat in 3-D format, and the three axes represent the information of light intensity, wavelength and scattering distance, respectively. The spectral range is between 400 nm to 1 100 nm, and the spatial distance is from -30 mm to 30 mm with the incident light center at 0 mm.

By resolving hyperspectral image spatially, the scattering profiles of pork meat at continuous wavelengths were obtained. The scattering profiles of pork meat at varying wavelengths were observed to be conspicuously similar in shape but with different light intensities. Therefore, it is reasonable to employ appropriate equations to analyze such light scattering pattern, and Gaussian, Exponential and Lorentzian functions were applied for this purpose. As an example, the scattering profiles of pork meat at the wavelengths of 500 nm, 600 nm, and 800 nm are shown in Figure 3.

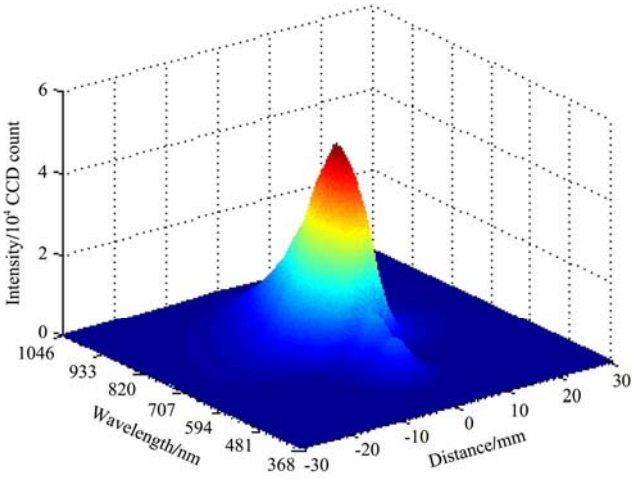

Figure 2 3-D hyperspectral image of pork meat

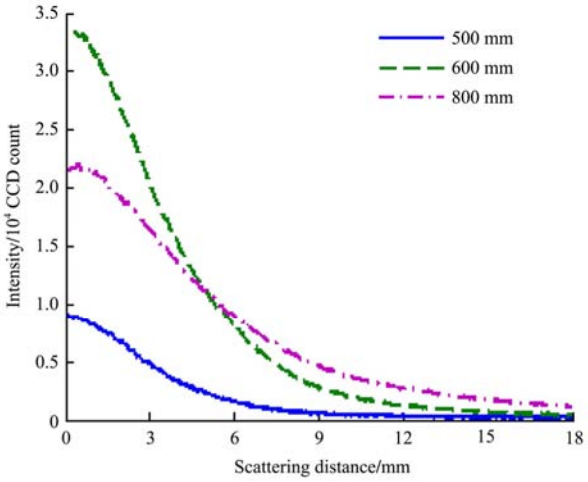

Figure 3 Scattering profiles at different wavelengths

3.2.2 Results of curve fitting and function parameters

Figure 4 shows the fitting coefficients of Gaussian, Exponential, and Lorentzian functions to the scattering profiles of pork meat in the selected spectral range. Overall, the fitting results by the three functions were good, with the fitting coefficients around 0.99 in the spectral range of 455-1 000 nm. In comparison, Lorentzian function fitted the scattering profiles of pork meat more accurately than Gaussian and Exponential functions, with all the fitting coefficients higher than 0.99. The result was in accordance with the study reported by Peng and Lu[29], in which they indicated that Lorentzian function was better than Gaussian and Exponential functions in fitting the multispectral scattering profiles of apple fruits.

Furthermore, in order to clearly show the comparison of the fitting results by Gaussian, Exponential and Lorentzian functions, the fitting coefficients of one scanning line were selected randomly and plotted in

Figure 5. From Figure 5, it could be seen that before 554 nm, the fitting coefficients by Gaussian function were similar to those by Lorentzian function, while inferior to Lorentzian function after 554 nm. Meanwhile, Gaussian function could fit the scattering profiles of pork meat more accurately than Exponential function between 455 nm and 600 nm, while inferior to Exponential function after 600 nm. In Peng and Lu's study[29] on modeling the multispectral scattering profiles of apple fruits, the fitting coefficients were in the descending sequence of Lorentzian function, Exponential function and Gaussian function.

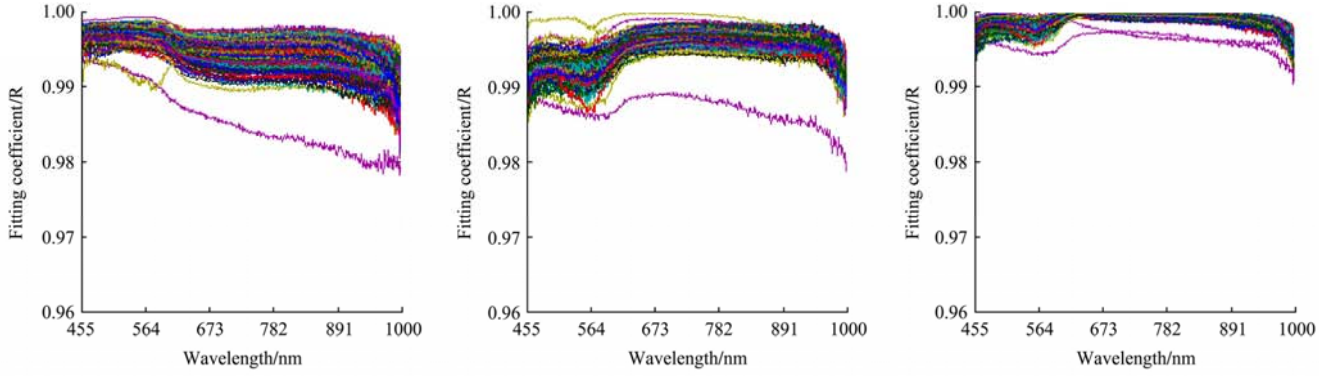

a. Gaussian function b. Exponential function c. Lorentzian function

Figure 4 Fitting coefficients by different functions:

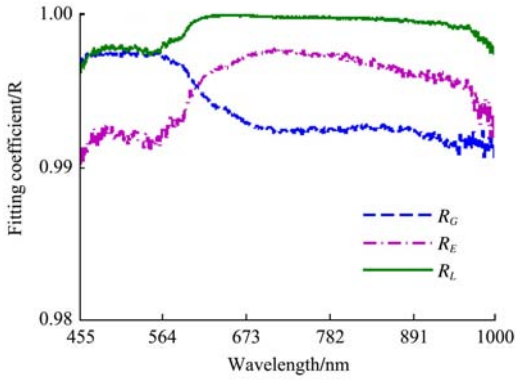

Figure 5 Fitting coefficients by three functions of one scanning line

Good fitting results indicate effective interpretation to the scattering profiles. Therefore, the derived function parameters could sufficiently represent the information within pork meat. Figures 6, 7 and 8 show the extracted Gaussian parameters, Exponential parameters, and Lorentzian parameters, respectively. It can be observed from Figures 6, 7 and 8 that the spectral patterns of the function parameters which represent the same meanings in the three functions are similar, while just with different magnitudes. In addition, it should also be noted that the spectral pattern of parameter a_G is in a unique type of similarity to parameters a_E and a_L, approximately being symmetric to parameters a_E and a_L with the horizontal axis.

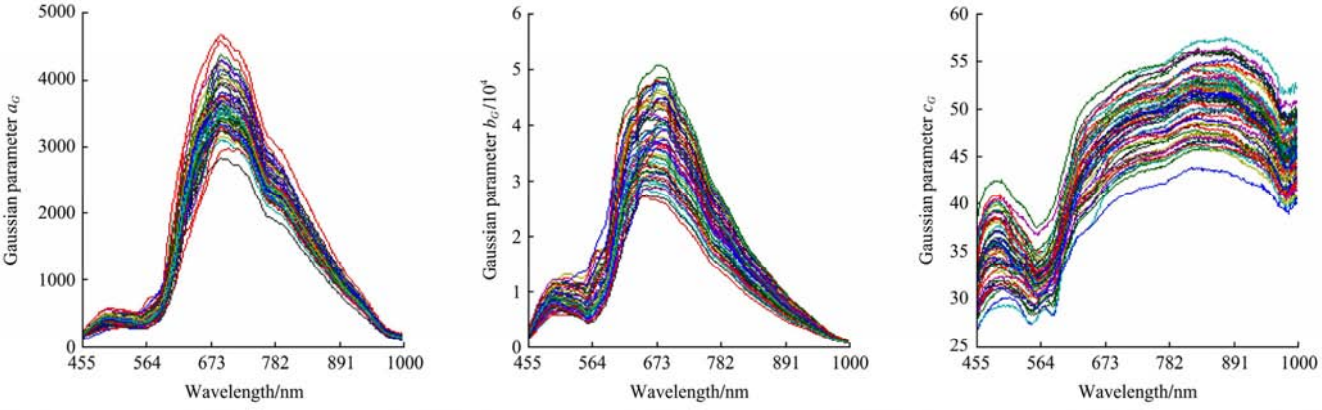

a. Parameter a_G b. Parameter b_G c. Parameter c_G

Figure 6 Gaussian parameters of 60 pork meat samples

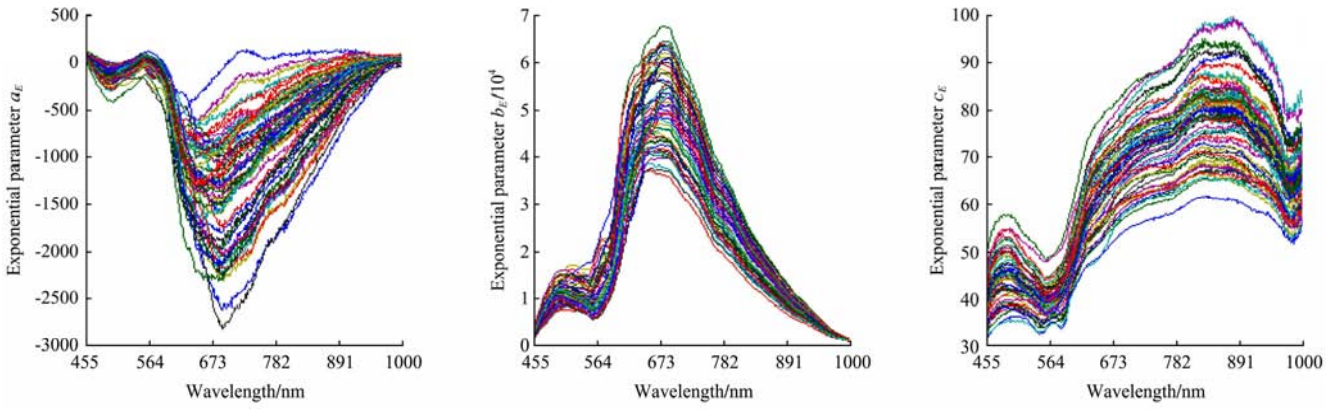

a. Parameter a_E b. Parameter b_E c. Parameter c_E

Figure 7 Exponential parameters of 60 pork meat samples

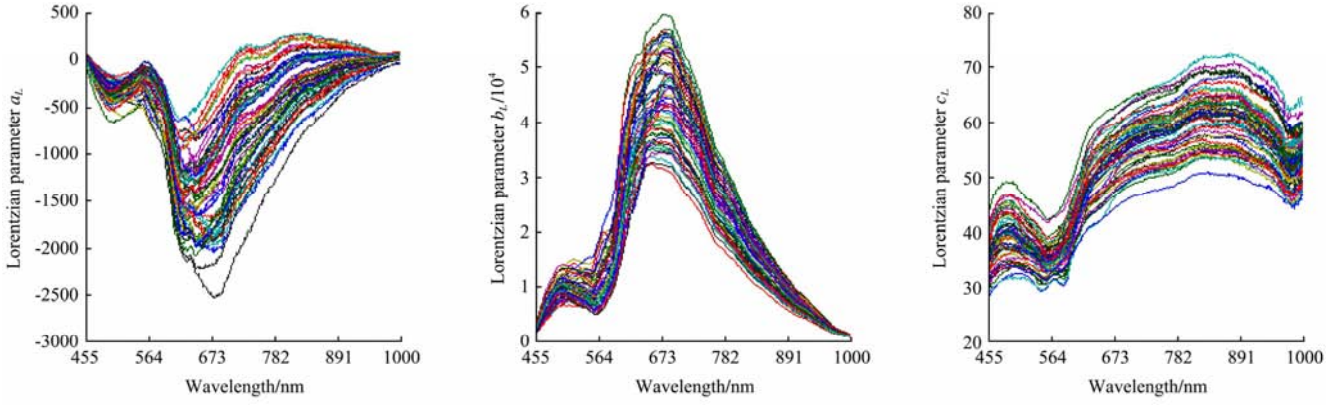

a. Parameter a_L b. Parameter b_L c. Parameter c_L

Figure 8 Lorentzian parameters of 60 pork meat samples

In detail, for parameters a_G, a_E and a_L, the spectral peaks and valleys were observed at the wavelengths of 500 nm, 551 nm, 635 nm and 680 nm, while they appeared around 510 nm, 546 nm, 571 nm and 663 nm for parameters b_G, b_E and b_L (Figures 6, 7 and 8). As to parameters c_G, c_E and c_L, it can be seen from their spectra that a wide spectral peak appeared after 600 nm approximately, except for the peaks and valleys around 494, 550 and 576 nm. Bowen[38] reported that the phenomenon of myoglobin oxidation would decrease the absorbance value at 555 nm, while increase around the wavelengths of 542 nm and 578 nm. These characteristic wavelengths reported are near the wavelengths mentioned above that showing peaks or valleys in the parameter spectra, which indicates that the phenomenon of myoglobin oxidation underwent during pork meat storage.

3.2.3 Correlation analysis between function parameters and pork meat TVC

In order to study the linear relationships between the extracted Gaussian, Exponential, Lorentzian parameters and pork meat TVC, the Pearson correlation coefficients (R) were calculated between 455 nm and 1 000 nm. Figure 9 shows the correlation coefficients between each function parameter and pork meat TVC, respectively. For parameters a_E and a_L, the correlation patterns with pork meat TVC were similar, while different with parameter a_G, which might result from their different parameter patterns (Figures 6a, 7a and 8a). The correlation patterns for parameters b and c were pretty similar for all the three functions, especially for parameters b_G, b_E and b_L, which were almost coincident in the selected spectral range. For parameters c_G, c_E and c_L, there was no obvious correlation difference with pork meat TVC before 596 nm, but the difference became notable after 596 nm, in the descending sequence of c_G, c_E and c_L.

In detail, the correlation coefficients of parameters a_G, a_E and a_L ranged from -0.75 to 0.62, while a_E and a_L correlating better to pork meat TVC than parameter a_G. Compared to parameter a, the correlation coefficients of

parameter *b* showed a little narrow range with the data varying from -0.56 to 0.44. The coefficients for parameter *c* were almost positive in the selected spectral range, with the highest coefficient of 0.73.

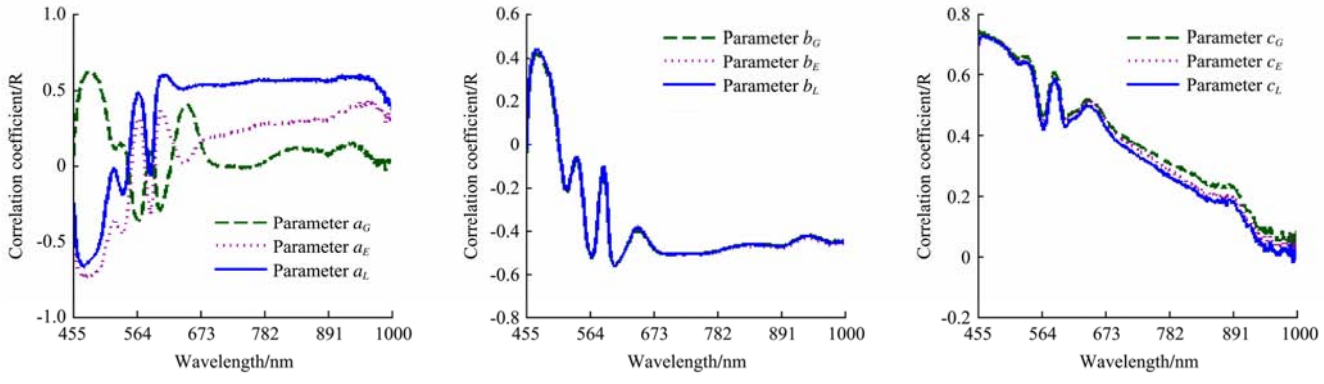

a. Parameter *a* b. Parameter *b* c. Parameter *c*

Figure 9 Correlation coefficients between pork meat TVC and function parameters

3.3 Modeling results for prediction of pork meat TVC

As mentioned above, both PCR and PLSR methods were applied to establish the prediction models. First, the prediction residual error sum of squares (PRESS) and standard error of cross validation (SE_{CV}) were calculated to determine the optimum PCs and LVs for PCR and PLSR methods, respectively. The optimum number of PCs is the one that yields the minimum PRESS, and correspondingly the optimum number of LVs is the one that yields the minimum SE_{CV}. Using parameter a_G, the optimum number of PCs and LVs were determined to be 11 and 7. Then, based on the optimum PCs and LVs determined, the PCR and PLSR models were calibrated and validated. The validation results using parameter a_G were achieved with R_V and RMSEV of 0.88, 0.72 log CFU/g, and 0.83, 0.84 log CFU/g by PCR and PLSR methods, respectively. The results indicated that using parameter a_G, PCR method gave more accurate prediction result than PLSR method.

Similarly by performing the leave-one out cross validation method, the optimum PCs and LVs using parameters b_G and c_G were determined. Table 2 shows the PCR and PLSR modeling results using parameters b_G and c_G. Table 2 shows that among all modeling results using Gaussian parameters by PCR and PLSR methods, the best prediction result was achieved using parameter c_G by PCR method, with *R*v and RMSEV of 0.89 and 0.68 log CFU/g. Additionally, it could also be observed from Table 2 that PCR method performed better than PLSR method, whichever Gaussian parameter was used.

Table 3 shows the modeling results using Exponential parameters, by PCR and PLSR method, respectively. From Table 3, it could be seen that among all Exponential parameters, the best prediction result was achieved using parameter c_E by PLSR method, with *R*v and RMSEV of 0.92, 0.59 log CFU/g. Additionally, Table 3 also shows that using Exponential parameters, PLSR method performed better than PCR method except for parameter b_E, which was different from the modeling results using Gaussian parameters.

Table 4 shows the modeling results using Lorentzian parameters, by PCR and PLSR method, respectively. Among the three Lorentzian parameters, the best prediction result was achieved using parameter c_L by PLSR method, with *R*v and RMSEV of 0.91, 0.61 log CFU/g. Although the *R*v using parameter a_L by PCR method reached 0.92, the RMSEV (0.73 log CFU/g) was bigger than that obtained using c_L by PLSR method. Moreover, no significant differences of the modeling results by PCR and PLSR methods were observed from Table 4.

Overall, from all the modeling results shown in Tables 2, 3 and 4, we observed that parameter *c* which represented the scattering width in all three functions gave more accurate prediction results for pork meat TVC than the other two parameters, whether it was based on PCR or PLSR method. Additionally, by comparing the prediction results using the same parameters from different functions, it could be concluded that Lorentzian parameters were superior to Gaussian parameters and Exponential parameters on prediction of pork meat TVC.

Table 2 PCR and PLSR modeling results using Gaussian parameters

Parameter	PCR method					PLSR method				
	Optimum No. of PCs	R_C	RMSEC	R_V	RMSEV	Optimum No. of LVs	R_C	RMSEC	R_V	RMSEV
a_G	11	0.91	0.61	0.88	0.72	7	0.92	0.58	0.83	0.84
b_G	4	0.85	0.78	0.87	0.76	9	0.92	0.58	0.86	0.87
c_G	6	0.84	0.79	0.89	0.68	13	0.99	0.10	0.85	0.76

Table 3 PCR and PLSR modeling results using Exponential parameters

Parameter	PCR method					PLSR method				
	Optimum No. of PCs	R_C	RMSEC	R_V	RMSEV	Optimum No. of LVs	R_C	RMSEC	R_V	RMSEV
a_E	2	0.50	1.26	0.48	1.35	11	0.99	0.19	0.76	1.15
b_E	4	0.84	0.79	0.87	0.78	9	0.92	0.58	0.86	0.85
c_E	7	0.85	0.77	0.89	0.67	4	0.84	0.79	0.92	0.59

Table 4 PCR and PLSR modeling results using Lorentzian parameters

Parameter	PCR method					PLSR method				
	Optimum No. of PCs	R_C	RMSEC	R_V	RMSEV	Optimum No. of LVs	R_C	RMSEC	R_V	RMSEV
a_L	8	0.86	0.73	0.92	0.73	11	0.99	0.16	0.86	0.86
b_L	4	0.84	0.78	0.87	0.76	9	0.92	0.58	0.87	0.85
c_L	8	0.84	0.79	0.89	0.69	5	0.84	0.80	0.91	0.61

The results indicated that parameter c_L performed best among the three Lorentzian parameters based on PCR or PLSR method, which was different from our previous study in which parameter b_L performed the best[25]. The system improvement should be the first important reason for the result differences. Moreover, different modeling methods may also lead to different modeling results, as stepwise multiple linear regression (SMLR) method was employed in our previous study, and PCR and PLSR methods were used in this work.

4 Conclusions

The study demonstrated that hyperspectral scattering imaging in tandem with appropriate chemometric methods could be a rapid and nondestructive tool for prediction of pork meat TVC. Gaussian, Exponential and Lorentzian functions were applied to model the hyperspectral scattering profiles of pork meat, and the results indicated that all the employed functions could fit the hyperspectral scattering profiles well, with the fitting coefficients around 0.99 between 455 and 1 000 nm. In comparison, Lorentzian function performed best in fitting the scattering profiles of pork meat.

Using the extracted function parameters, both PCR and PLSR methods were performed to develop the quantitative models for prediction of pork meat TVC. Among all the established models, the models developed using parameters c_E and c_L by PLSR method gave superior results, with Rv and RMSEV of 0.92 and 0.59 log CFU/g, 0.91 and 0.61 log CFU/g, respectively. In addition, this study showed that based on the improved hyperspectral scattering system, parameter c which represented the scattering width in all three functions gave more accurate results in predicting pork meat TVC than the other two function parameters, regardless of the modeling method (PCR or PLSR). Overall, the study demonstrated that hyperspectral scattering imaging combined with the presented data analysis algorithm could be a powerful tool for evaluating the microbial safety of meat in the future.

Acknowledgements

The authors gratefully acknowledge the China Postdoctoral Science Foundation (Project No. 2014M561096), the Special Fund for Agro-scientific Research in the Public Interest Program (Project No. 201003008), and the National Science and Technology Support Program (Project No. 2012BAH04B00) for supporting this research.

[References]

[1] Sofos J N. Challenges to meat safety in the 21st century. Meat Science, 2008; 78(1-2): 3−13.

[2] Nychas G-J E, Skandamis P N, Tassou C C, Koutsoumanis K P. Meat spoilage during distribution. Meat Science, 2008; 78(1-2): 77−89.

[3] China National Standard. GB2707-2005 Hygienic standard for fresh (frozen) meat of livestock. Standards Press of China, 2005.

[4] Commission E. Commission regulation (EC) no 2073/2005 of November 2005 on microbiological criteria for foodstuffs (text with EEA relevance). Official Journal of the European Union, 2005; L338/1 − L338/26.

[5] Borch E, Kant-Muermans M L, Blixt Y. Bacterial spoilage of meat and cured meat products. International Journal of Food Microbiology, 1996; 33(1): 103−120.

[6] Dainty R H. Chemical/biochemical detection of spoilage. International Journal of Food Microbiology, 1996; 33(1): 19−33.

[7] Ellis D I, Goodacre R. Rapid and quantitative detection of the microbial spoilage of muscle foods: Current status and future trends. Trends in Food Science and Technology, 2001; 12(11): 414−424.

[8] Ellis D I, Broadhurst D, Kell D B, Rowland J J, Goodacre R. Rapid and quantitative detection of the microbial spoilage of meat by Fourier transform infrared spectroscopy and machine learning. Applied and Environmental Microbiology, 2002; 68(6): 2822−2828.

[9] Barbri N E, Llobet E, Bari N E, Correig X, Bouchikhi B. Electronic nose based on metal oxide semiconductor sensors as an alternative technique for the spoilage classification of red meat. Sensors, 2008; 8: 142−156.

[10] Shackelford S D, Wheeler T L, Koohmaraie M. Tenderness classification of beef: II, design and analysis of a system to measure beef longissimus shear force under commercial processing conditions. Journal of Animal Science, 1999; 77(6): 1474−1481.

[11] Vote D J, Belk K E, Tatum J D, Scanga J A, Smith G C. Online prediction of beef tenderness using a computer vision system equipped with a BeefCam module. Journal of Animal Science, 2003; 81(2): 457−465.

[12] Barbin D F, ElMasry G, Sun D-W, Allen P, Morsy N. Non-destructive assessment of microbial contamination in porcine meat using NIR hyperspectral imaging. Innovative Food Science and Emerging Technologies, 2013; 17: 180−191.

[13] ElMasry G, Iqbal A, Sun D-W, Allen P, Ward P. Quality classification of cooked, sliced turkey hams using NIR hyperspectral imaging system. Journal of Food Engineering, 2011; 103(3): 333−344.

[14] Feng Y Z, Sun D-W. Determination of total viable count (TVC) in chicken breast fillets by near-infrared hyperspectral imaging and spectroscopic transforms. Talanta, 2013; 105: 244−249.

[15] Park B, Lawrence K C, Windham W R, Buhr R J. Hyperspectral imaging for detecting fecal and ingesta contaminants on poultry carcasses. Transactions of the ASABE, 2002; 45(6): 2017−2026.

[16] Park B, Lawrence K C, Windham W R, Smith D. Performance of hyperspectral imaging system for poultry surface fecal contaminant detection. Journal of Food Engineering, 2006; 75: 340−348.

[17] Peng Y K, Lu R. Analysis of spatially resolved hyperspectral scattering images for assessing apple fruit firmness and soluble solids content. Postharvest Biology and Technology, 2008; 48(1): 52−62.

[18] Peng Y K, Zhang J, Wang W, Li Y Y, Wu J H, Huang H, et al. Potential prediction of the microbial spoilage of beef using spatially resolved hyperspectral scattering profiles. Journal of Food Engineering, 2011; 102(2): 163−169.

[19] Qiao J, Ngadi M O, Wang N, Gariepy C, Prasher S O. Pork quality and marbling level assessment using a hyperspectral imaging system. Journal of Food Engineering, 2007; 83(1): 10−16.

[20] Talens P, Mora L, Morsy N, Barbin D F, ElMasry G, Sun D W. Prediction of water and protein contents and quality classification of Spanish cooked ham using NIR hyperspectral imaging. Journal of Food Engineering, 2013; 11(3)7: 272−280.

[21] Tao F F, Wang W, Li Y Y, Peng Y K, Wu J H, Shan J J, et al. A rapid nondestructive measurement method for assessing the total plate count on chilled pork surface. Spectroscopy and Spectral Analysis, 2010; 30(12): 3405−3409.

[22] Tao F F, Peng Y K, Li Y Y, Chao K, Dhakal S. Simultaneous determination of tenderness and Escherichia coli contamination of pork using hyperspectral scattering technique. Meat Science, 2012; 90(3): 851−857.

[23] Tao F F, Tang X, Peng Y K, Dhakal S. Classification of pork quality characteristics by hyperspectral scattering technique. In: Symposium Conducted at ASABE Annual International Meeting, Dallas, Texas, USA, 2012.

[24] Tao F F, Peng Y K. A method for nondestructive prediction of pork meat quality and safety attributes by hyperspectral imaging technique. Journal of Food Engineering, 2014; 126: 98−106.

[25] Tao F F, Peng Y K. A nondestructive method for prediction of total viable count in pork meat by hyperspectral scattering imaging. Food and Bioprocess Technology, 2015; 8(1): 17−30.

[26] Wu J H, Peng Y K, Li Y Y, Wang W, Chen J, Dhakal S.

Prediction of beef quality attributes using VIS/NIR hyperspectral scattering imaging technique. Journal of Food Engineering, 2012; 109(2): 267−273.

[27] Zhang L L, Peng Y K, Tao F F, Zhao S W, Song Y L. Rapid non-destructive detection of total volatile basic nitrogen in pork using hyperspectral technique. Journal of Food Safety and Quality, 2012; 3(6): 575−579.

[28] Guo Z, Huang W, Chen L, Peng Y K, Wang X. Shortwave infrared hyperspectral imaging for detection of pH value in Fuji apple. Int J Agric & Biol Eng, 2014; 7(2): 130−137.

[29] Peng Y, Lu R. Modeling multispectral scattering profiles for prediction of apple fruit firmness. Transactions of the ASAE, 2005; 48(1): 235−242.

[30] Peng Y K, Lu R. Prediction of apple fruit firmness and soluble solids content using characteristics of multispectral scattering images. Journal of Food Engineering, 2007; 82(2): 142−152.

[31] Zhu Q, Huang M, Zhao X, Lu R. Analysis of hyperspectral scattering profiles using generalized Gaussian distribution for prediction of apple firmness and soluble solids content. In: Symposium Conducted at ASABE Annual International Meeting, Louisville, Kentucky, USA, 2011.

[32] Beebe K R, Kowalski B R, Wold H. An introduction to multivariate calibration and analysis. Analytical Chemistry, 1987; 59: 1007A−1017A.

[33] Goodacre R, Timmins E M, Burton R, Kaderbhai R, Woodward A M, Kell D B. Rapid identification of urinary tract infection bacteria using hyperspectral whole-organism fingerprinting and artificial neural networks. Microbiology, 1998; 144: 1157−1170.

[34] Haaland D M, Thomas E V. Partial least-squares methods for spectral analyses, Relation to other quantitative calibration methods and the extraction of qualitative information. Analytical Chemistry, 1988; 60: 1193−1202.

[35] Haaland D M, Thomas E V. Comparison of multivariate calibration methods for quantitative spectral analysis. Analytical Chemistry, 1990; 62(10): 1091−1099.

[36] Martens H, Naes T. Multivariate Calibration, 1989; second ed., John Wiley & Sons, Ltd., Chichester, United Kingdom.

[37] Park B, Abbott J A, Lee K J, Choi C H, Choi K H. Near-infrared diffuse reflectance for quantitative and qualitative measurement of soluble solids and firmness of delicious and gala apples. Transactions of the ASAE, 2003; 46(2): 1721−1731.

[38] Bowen W J. The absorption spectra and extinction coefficients of myoglobin. Journal of Biological Chemistry, 1949; 179(1): 235−245.